Chapter 4
Improving the Resiliency of a PV Stand-Alone with Energy Storage

4.1 Introduction

The stand-alone PV system is controlled using MPPT algorithm under the impact of the fixed or changing solar irradiation, and the system is connected to BES to produce power for variable AC loads. The system comprises of PV array, BES, DC/DC boost converter circuit, single-phase inverter with LCL filter, and bidirectional DC/DC buck-boost converter performing as charging circuit. The MPP be able to obtain by controlling the duty cycle fed to the gate of the IGBT transistor located within the boost circuit. Moreover, the control method used with both the single-phase inverter and the buck-boost converter circuit is a dynamic error driven PI controller.

This chapter investigates a dynamic modeling, simulation, and control strategy of the proposed PV stand-alone system with BES. Moreover, this chapter discusses the performance comparison of PV stand-alone system with BES in two cases of operation. In the first case, the system operates without and with BES under constant solar irradiation. In the second case, the PV system is connected to a BES and operates under a variable in solar irradiation. In addition to presenting the operating results of the system for the two cases mentioned previously, harmonic analysis is performed on these results using the fast Fourier transform (FFT) tools.

4.2 Structure and Modeling a PV Stand-Alone with Battery Energy Storage

The objective of this section is to design an independent PV system containing a PV panel, DC/DC boost converter, and half-bridge buck-boost bidirectional chopper and focuses on increasing energy extraction by improving MPPT. The P&O MPPT technique is implemented on the DC/DC boost converter to extract the maximum

A. A. Elbaset et al., *Performance Analysis of Photovoltaic Systems with Energy Storage Systems*, https://doi.org/10.1007/978-3-030-20896-7_4

power from the PV station during variation of the solar irradiance. The system is rated to 5 kW generated by PV array and Two loads; each of 3 kW can be connected to the DC/AC inverter. This makes the overall electrical power consumed 6 kW when both are connected. Figure 4.1 clarifies the simplified diagram of the stand-alone PV system with BES. The mathematical model for each of the system components is described in the following subsections.

4.2.1 Mathematical Modeling of the PV Array Under Study

The studied PV array is formed by connecting a number of 4 PV strings in parallel in order to increase the output current and achieve the array rated power (P_{array} = 5040 W). The PV string is composed by connecting number of 6 PV modules in series to increase the output voltage at the MPP (V_{mpp} = 202.8 V). Figure 4.2 shows the electrical modeling of the PV array based on the Shockley diode. Also, the implementation of the PV array in MATLAB/Simulink model is depicted in

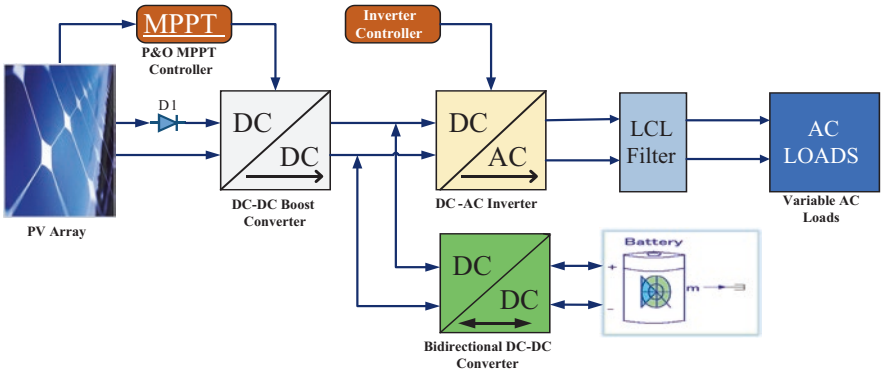

Fig. 4.1 Simplified diagram of the stand-alone photoelectric system with energy storage

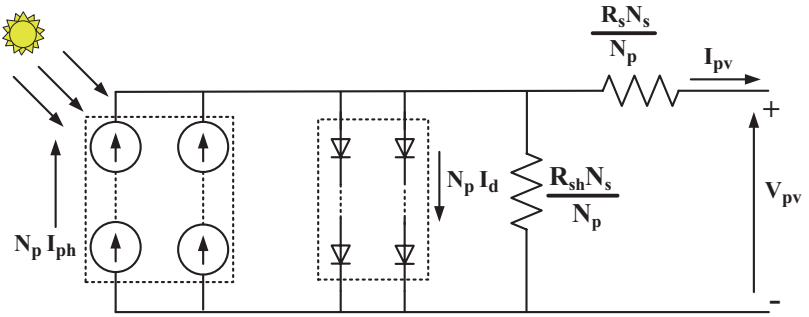

Fig. 4.2 The electrical model of the PV array

Fig. 4.3. The electrical characteristics of the PV array can be simulated with regard to the variations in the environmental conditions such as the solar irradiance intensity and temperature.

The current-voltage (I-V) characteristics and the power-voltage (P-V) characteristics of the employed PV array during variation of the solar irradiance and the corresponding current-voltage (I-V) relationship of the PV array have been introduced and reviewed in Sect. 2.3.1. Furthermore, the detailed specifications of the studied PV array are listed in Table 4.1.

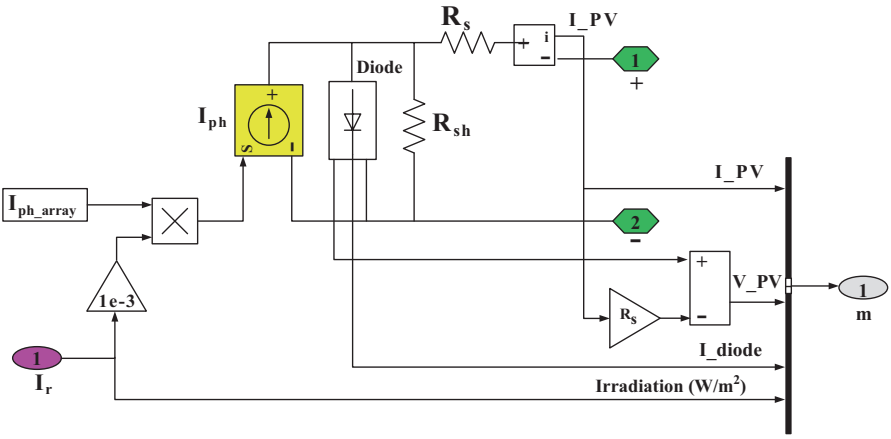

Fig. 4.3 MATLAB/Simulink model of the PV array

Table 4.1 Design parameters of the PV array

Design parameter	Symbol	Value
Module type	Solaria Solaria 210	
Rated power of PV module	$P_{PV-module}$	209.96 W
Number of cells per module	N_{ser}	70
Number of parallel strings	N_P	4
Number of series-connected modules	N_S	6
Light-generated current	I_{pv}	7.1774 A
PV saturation current	I_s	0.27907 nA
Series resistance	R_s	0.40587 Ω
Parallel resistance	R_{sh}	55.9684 Ω
Maximum power per array	p_{array}	5040 W
Voltage at maximum power point of PV array	V_{mpp}	202.8 V
Current at maximum power point of PV array	I_{mpp}	24.852 A
Open-circuit voltage of PV module	V_{oc}	41.59 V
Short-circuit current of PV module	I_{sc}	7.13 A

4.2.2 DC/DC Boost Converter

Two-stage topology selected for the DC-DC chopper in PV system takes care of MPPT. The employment of two-stage topology allows the system to be customizable, i.e., it can be transformed to a multi-string system to increase the capacity of the system in the future, with each series having its own MPPT and DC/DC boost converter. This was about the significance of the DC/DC converter, but the configuration is illustrated in Fig. 4.4.

As shown in Fig. 4.4, the MPPT technique is implemented on the DC/DC boost converter to capture the maximum power from the PV array during variation of the solar irradiance. Therefore, the switching duty cycle of the DC/DC boost converter is generated by the P&O MPPT technique [71]. Also, the design parameters of the DC/DC boost converter were calculated using the equations shown in Sect. 2.3.2, which are listed in Table 4.2.

4.2.3 Single-Phase DC/AC Inverter

Inverters are circuits that convert DC to AC. More precisely, inverters transfer power from a DC source to an AC load. The controlled full-wave bridge converters can function as inverters in some instances, but an AC source must preexist in those cases. In other applications, the objective is to create an AC voltage when only a DC

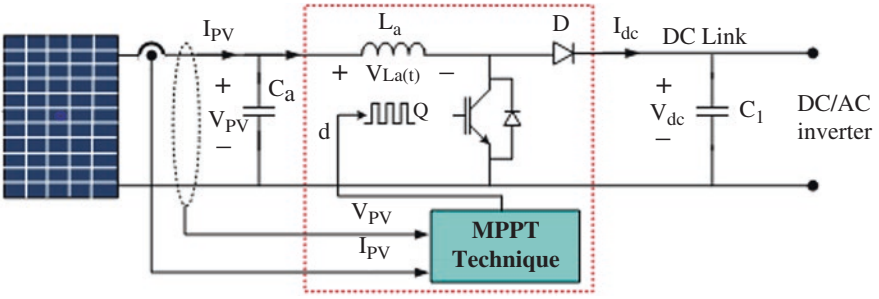

Fig. 4.4 The PV array with the DC/DC boost converter

Table 4.2 Design parameters of the DC/DC boost converter

Design parameter	Symbol	Value
Input capacitance	C_a	1 mF
Inductance of boost converter	L_a	240 μH
Output capacitance	C_1	5 mF
Switching frequency	f_s	10 kHz
Output voltage	V_{dc}	280 V

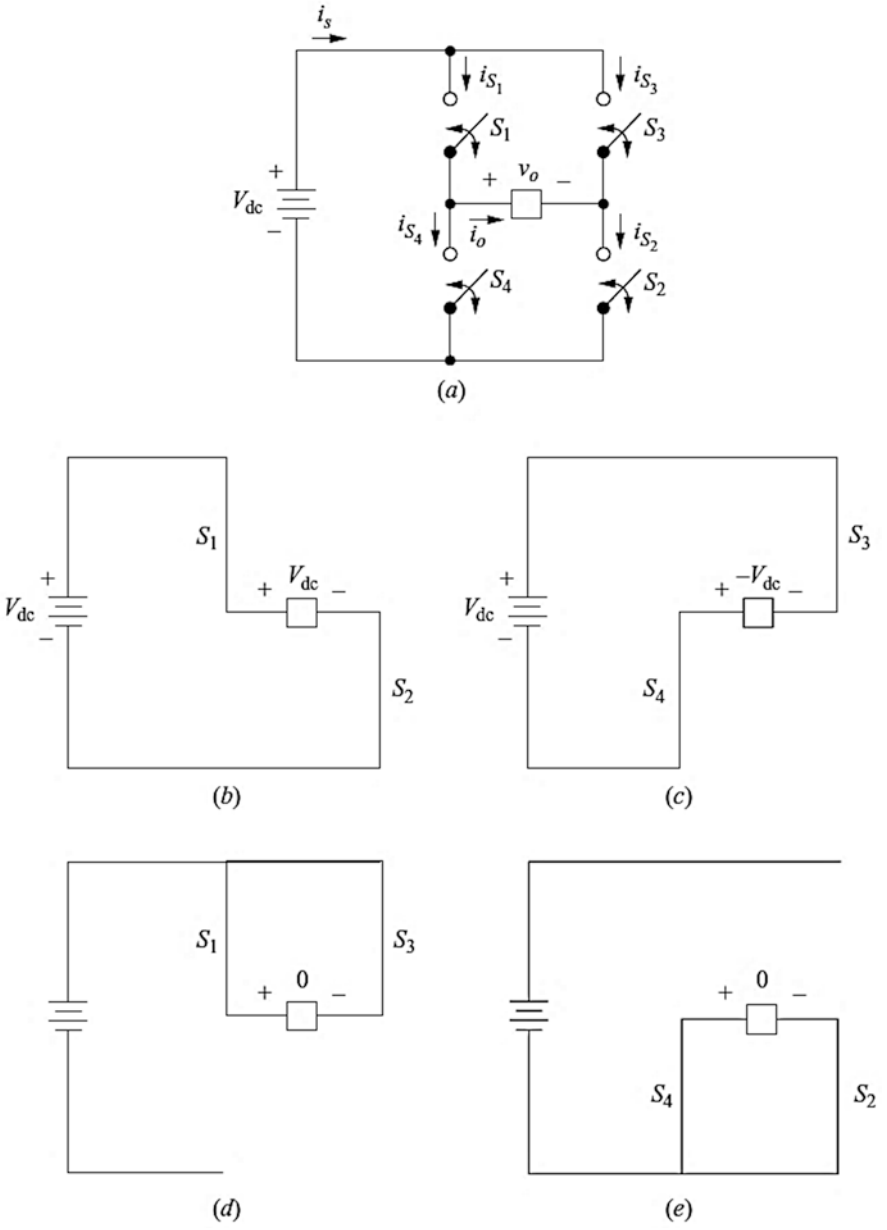

Fig. 4.5 (**a**) Full-bridge converter; (**b**) S1 and S2 closed; (**c**) S3 and S4 closed; (**d**) S1 and S3 closed; (**e**) S2 and S4 closed

voltage source is available. The focus of this section is on single-phase inverters that produce an AC output from a DC input. Inverters are used in applications such as adjustable-speed AC motor drives, uninterruptible power supplies, PV systems, and running AC appliances from an automobile BES. Inverters are power electronic devices used in various PV system configurations [24, 74]:

- Grid-connected systems
- Stand-alone systems with rechargeable batteries
- Pumping systems without storage batteries

The full-bridge converter of Fig. 4.5a is the basic circuit used to convert DC to AC. In this circuit, an AC output is synthesized from a DC input by closing and opening the switches in an appropriate sequence. The output voltage V_O can be $+V_{dc}$, $-V_{dc}$, or zero, depending on which switches are closed. Figure 4.5b–e shows the equivalent circuits for switch combinations. Note that S_1 and S_4 should not be closed at the same time nor should S_2 and S_3. Otherwise, a short circuit would exist across the DC source. Real switches do not turn on or off instantaneously. Therefore, switching transition times must be accommodated in the control of the switches. Overlap of switch "on" times will result in a short circuit, sometimes called a shoot-through fault, across the DC voltage source. The time allowed for switching is called blanking time [69] (Table 4.3).

The power quality required for loads must match the quality of the power produced by the inverter. Therefore, there are different types of inverters. The function of the inverter is to attach the systems to each other and supply the PV energy in the network as efficiently as possible. For the required square wave voltage, a simple control strategy is employed to obtain the inverter switch signals, which are turned on and off at AC frequency and consist of high consistent currents and voltages. The control method used is dynamic error-driven PI controller as shown in Fig. 4.6 where its input is the error signal resulting from the difference between the V_{dc} of the boost converter and the reference voltage ($V_{ref} = 280V$). The control signal generated by the PI controller is adjusted to be a value in the range (-1 to 1) in order to match with a sine wave generated by sine wave (V_{ref}) generation. This gives a 60 Hz frequency control signal then utilized as the modulation index for the pulse width modulation generator to get the switching control signals.

The power that is used by converters is very significant in increasing the transport of power from PV energy system to the grid or AC loads. The harmonic results due to the operation of power electronic converters. The harmonic voltage and current ought to be restricted to the acceptable level for the point of PV generator link

Table 4.3 Switches cases of full-bridge inverter

Switches closed	Output voltage V_O
S1 and S2	$+V_O$
S3 and S4	$-V_O$
S1 and S3	0
S2 and S4	0

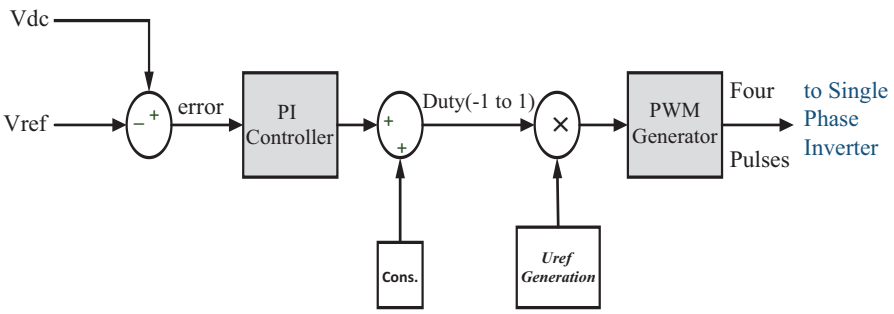

Fig. 4.6 The dynamic error-driven PI controller for the DC-AC inverter

to the networks and electrical loads. To ensure the harmonic voltage within the limit, each method of obtaining harmonic current can allow only a limited contribution, as per the international standard guideline. The filter must be used to reduce the total harmonics in AC voltage and current.

4.2.4 Filter Design

Recently, the development of renewable energy technologies has been accelerating, making the simultaneous development of power conversion devices for applications, such as wind and PV systems, extremely important; the development of these technologies is actively underway. The harmonics caused by the switching of the power conversion devices are the main factor-causing problems to sensitive equipment or the connected loads, especially for applications above several kilowatts, where the price of filters and total harmonics distortion (THD) is also an important consideration in the systems design phase [75]. The inductance of the input or output circuits of the power conversion devices has conventionally been used to reduce these harmonics. However, as the capacity of the systems has been increasing, high values of inductances are needed, so that realizing practical filters has been becoming even more difficult due to the price rises and the poor dynamic responses.

An L filter or LCL filter is usually placed between the inverter and the grid to attenuate the switching frequency harmonics produced by the grid-connected inverter. Compared with L filter, LCL filter has better attenuation capacity of high-order harmonics and better dynamic characteristic. However, an LCL filter can cause stability problems due to the undesired resonance caused by zero impedance at certain frequencies. To avoid this resonance from contaminating the system, several damping techniques have been proposed. One way is to incorporate a physical passive element, such as a resistor in series with the filter capacitor [76]. This passive damping solution is very simple and highly reliable. However, the additional resistor results in power loss and weakens the attenuation ability of the LCL filter. This drawback can be overcome by employing active damping (Figs. 4.7 and 4.8).

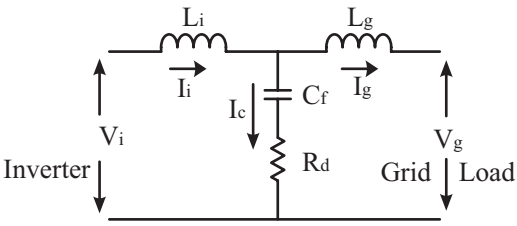

Fig. 4.7 LCL filter and components

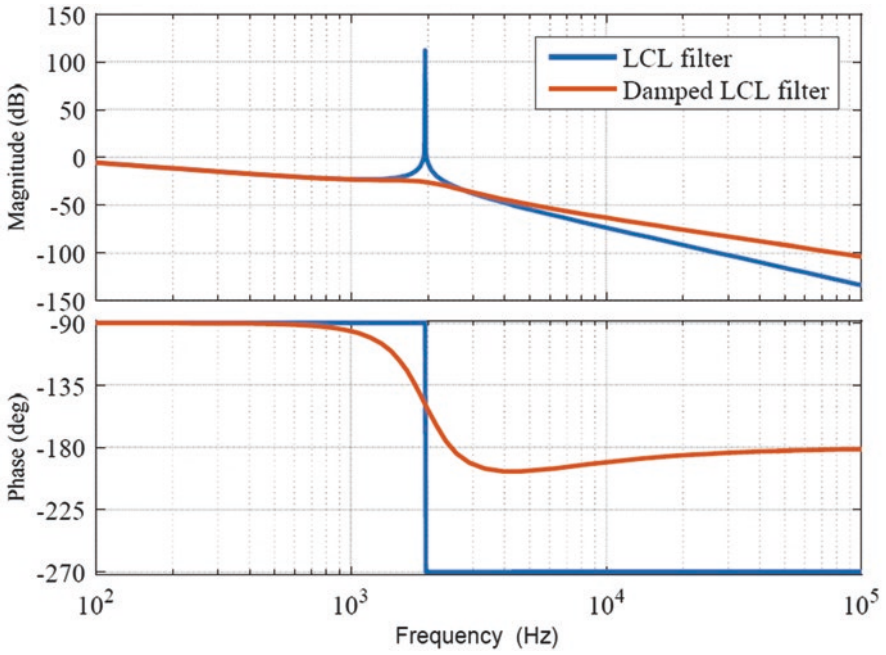

Fig. 4.8 LCL filter with passive damping resistance [79]

The cutoff frequency (f_{res}) must have a sufficient distance from the grid frequency or the connected electrical AC loads. The cutoff frequency (f_{res}) of the LCL filter can be calculated as [77]

$$f_{res} = \frac{1}{2\pi} \times \sqrt{\frac{L_i + L_g}{L_i \times L_g \times C_f}} \tag{4.1}$$

The LCL filter will be vulnerable to oscillations and it will magnify frequencies around its cutoff frequency (f_{res}). Therefore, the filter is added with damping. The simplest way is to add damping resistor (R_d). The variant with resistor connected in series with the filter capacitor has been chosen. The passive damped LCL filter frequency response is shown in Fig. 4.9. However, it is obvious that the damping

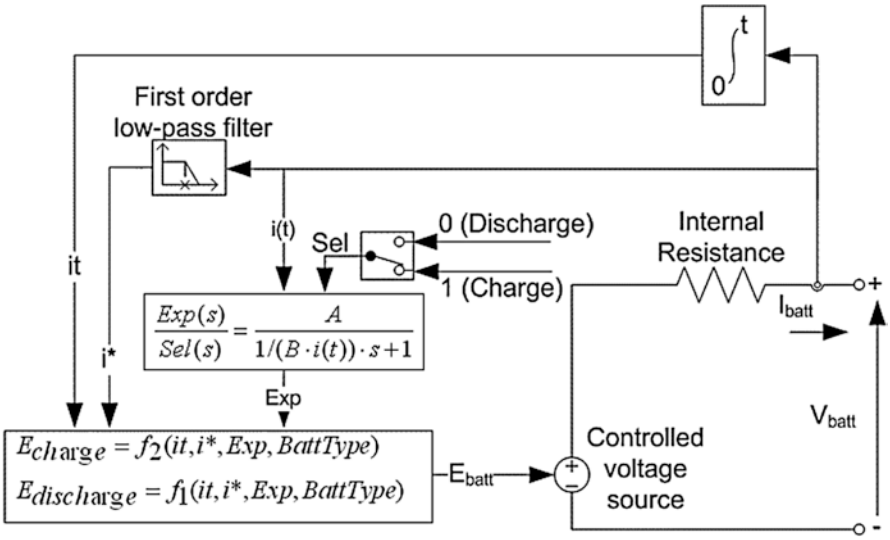

Fig. 4.9 The equivalent circuit of battery [81]

resistor reduces the efficiency of the overall system. The value of the damping resistor (R_d) can be calculated as [78]

$$R_d = \frac{1}{3\omega_{res} C_f} \tag{4.2}$$

The following parameters are needed for the filter design:

U_n, line-to-line RMS voltage (inverter output); P_n, rated active power; V_{dc}, DC link voltage; f_n, grid frequency; f_s, switching frequency. Thus, the filter values will be referred to in a percentage of the base values [79]:

$$Z_b = \frac{U_n^2}{P_n} \tag{4.3}$$

$$C_b = \frac{1}{\omega_n Z_b} \tag{4.4}$$

The first step in calculating the filter components is the design of the inverter side inductance (L_i), which can limit the output current ripple by up to 10% of the nominal amplitude. It can be calculated according to the equation derived in

$$L_i = \frac{V_{dc}}{16 f_s \Delta I_L} \tag{4.5}$$

where ΔI_L is the 10% current ripple specified by

$$\Delta I_L = 0.01 \frac{P_n \sqrt{2}}{U_n} \tag{4.6}$$

The design of the filter capacity proceeds from the fact that the maximal power factor variation acceptable by the grid is 5%. The filter capacity can be calculated as a multiplication of system base capacitance (C_b):

$$C_f = 0.05 C_b \tag{4.7}$$

The grid side inductance (L_g) can be calculated as

$$L_g = r * L_i \tag{4.8}$$

where (r) is the factor between (L_i) and (L_g). The M-file program in MATLAB calculates the value of each component of the LCL filter found in Appendix B.

4.2.5 Modeling of Battery Energy Storage

The BES is used to store solar energy whenever it is available in excess. Stored energy is used when PV energy is not enough to afford load demand. In addition, a complete review of the types of batteries used with PV systems was conducted in the third chapter. The focus was also on the type of lead-acid batteries. In this book, the BES is used from lead-acid type because it is more proper for renewable systems because of its limited cost and availability in large volume. Today lead-acid batteries are the best effectual solution for independent renewable energy systems because of their low cost, deep cycling, high discharges, and recycling. The BES block implements a generic dynamic model parameterized to represent most popular types of rechargeable batteries. The Fig. 4.9 shows the BES equivalent circuit that the block models [80].

In this section, lead-acid BES model is implemented using Simulink. The corresponding equations for charge and discharge model are represented according to the following equations [14]:

Charge model ($i* < 0$)

$$f_2\left(\text{it}, i^*, i, \text{Exp}\right) = E_0 - K \cdot \frac{Q_b}{\text{it} + 0.1 \cdot Q_b} \cdot i^* - K \cdot \frac{Q_b}{Q_b - \text{it}} \cdot \text{it} + \text{Laplace}^{-1}\left(\frac{\text{Exp}(s)}{\text{Sel}(s)} \cdot \frac{1}{s}\right) \tag{4.9}$$

Discharge model ($i* > 0$)

$$f_1\left(\text{it},i^*,i,\text{Exp}\right) = E_0 - K\cdot\frac{Q_b}{\text{it}+0.1\cdot Q_b}\cdot i^* - K\cdot\frac{Q_b}{Q_b-\text{it}}\cdot\text{it} + \text{Laplace}^{-1}\left(\frac{\text{Exp}(s)}{\text{Sel}(s)}\cdot 0\right) \quad (4.10)$$

where

i The battery current (A)
$i*$ The low-frequency current dynamics (A)
it The extracted capacity (Ah)
Exp(s) Exponential zone dynamics (V)
E_0 The constant voltage (V)
K The polarization constant (Ah^{-1}) or polarization resistance (Ω)
Q_b Maximum battery capacity (Ah)
Sel(s) Represents the battery mode. Sel(s) = 0 during battery discharge, Sel(s) = 1 during battery charging

The BES discharge characteristics typical curve is consisting of three sections as shown in Fig. 4.10. The first section represents the exponential voltage drop when the BES is charged. The width of the drop depends on the BES type. The second section represents the charge that can be extracted from the BES until the voltage drops below the battery nominal voltage. The third section represents the total discharge of the BES, when the voltage drops rapidly.

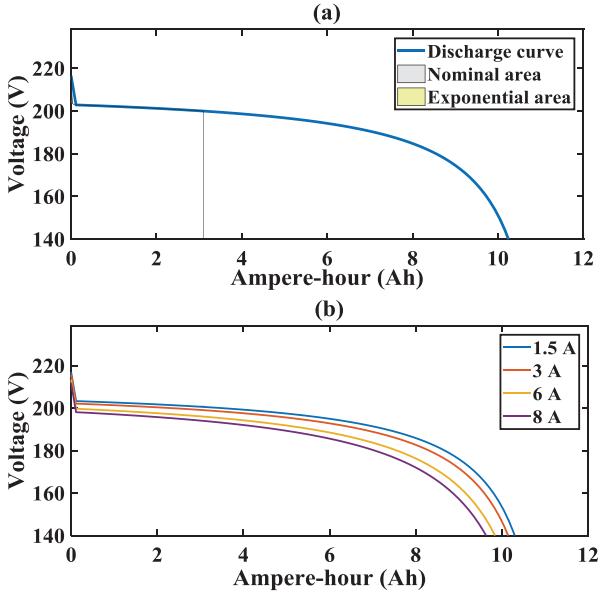

Fig. 4.10 Discharge characteristics of a lead-acid battery. (**a**) Nominal current discharge characteristic at (2A). (**b**) Discharge characteristic at diverse current values

4.2.6 Half-Bridge Bidirectional DC/DC Buck/Boost Converter

Bidirectional DC/DC converters serves the purpose of stepping up or stepping down the voltage level between its input and output along with the capability of power flow in both directions. Bidirectional DC/DC converters have attracted a great deal of applications in the area of the energy storage systems for hybrid vehicles, renewable energy storage systems, uninterruptable power supplies, and fuel cell storage systems. Bidirectional DC/DC converters are employed when the DC bus voltage regulation must be achieved along with the power flow capability in both the directions. One such example is the power generation by wind or PV power systems, where there is a large fluctuation in the generated power because of the large variation and uncertainty of the energy supply to the conversion unit (PV array) by the primary source [82]. These systems cannot serve as a stand-alone system for power supply because of these large fluctuations and therefore these systems are always backed up and supported by the auxiliary sources which are rechargeable such as BES units or SCs. These sources supplement the main system at the time of energy deficit to provide the power at a regulated level and get recharged through the main system at the time of surplus power generation or at their lower threshold level of discharge. Bidirectional DC/DC converter is needed to be able to allow power flow in both the directions at the regulated level.

Likewise, in PV systems, bidirectional DC/DC converters are employed to link up the high-voltage DC bus to the hybrid energy storage system (usually a combination of the BES with the *SC*). Here they are needed to regulate the power supply for electrical loads to help them provide their power demanded. The bidirectional DC/DC converters can be classified into two categories depending on the galvanic isolation between the input and output side [83]:

- Non-isolated bidirectional DC/DC converters.
- Isolated bidirectional DC/DC converters.

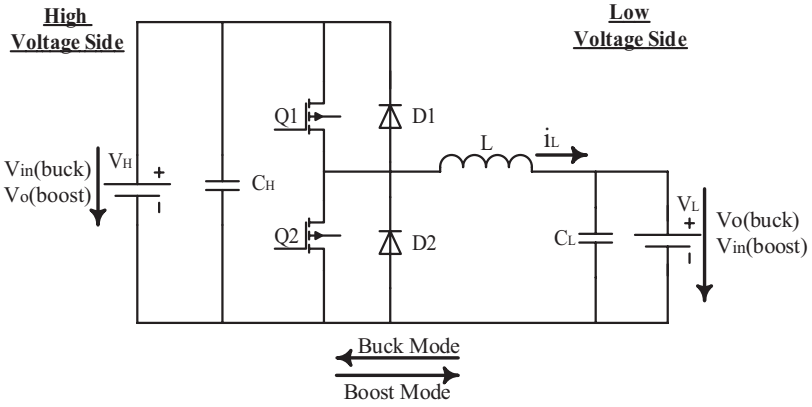

Fig. 4.11 Circuit diagram of half-bridge bidirectional DC/DC converter

In this book, the non-isolated bidirectional half-bridge DC/DC converters are used to connect the BES with the PV system, which illustrated its circuit diagram in Fig. 4.11. Basically, a non-isolated bidirectional DC/DC converter can be derived from the unidirectional DC/DC converters by enhancing the unidirectional conduction capability of the conventional converters by the bidirectional conducting switches. Due to the presence of the diode in the basic buck and boost converter circuits as shown in Fig. 4.12a, b, they do not have the inherent property of the bidirectional power flow. This limitation in the conventional boost and buck converter circuits can be removed by introducing a power MOSFET or an IGBT having an antiparallel diode across them to form a bidirectional switch and hence allowing current conduction in both directions for bidirectional power flow in accordance with the controlled switching operation as clarified in Fig. 4.11. When the Buck and the boost converters are connected in antiparallel across each other with the resulting circuit is basically having the same structure as the fundamental Boost and Buck structure but with the added feature of bidirectional power flow [58, 60].

The above circuit can be made to work in buck or boost mode depending on the switching of the switches Q1 and Q2. The switches Q1 and Q2 in combination with the antiparallel diodes D1 and D2 (acting as a freewheeling diode), respectively, make the circuit step up or step down the voltage applied across them. The bidirectional operation of the above circuit can be explained in the below two modes as follows:

Mode 1 (Boost Mode) In this mode, switch Q2 and diode D1 enter into conduction depending on the duty cycle, whereas the switch S1 and diode D2 are off all the time. This mode can further be divided into two intervals depending on the conduction on the switch 1 and diode D2 as shown in Fig. 4.12b.

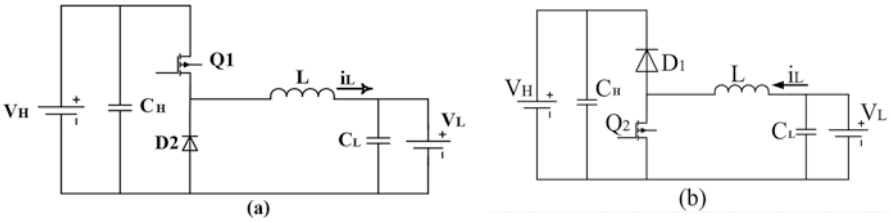

Fig. 4.12 (**a**) Buck converter circuit and (**b**) boost converter circuit

Interval 1 (Q2-on, D2-off; Q1-off, D2-off) In this mode Fig. 4.13a, Q2 is on and hence can be considered to be short-circuited; therefore, the lower-voltage battery charges the inductor, and the inductor current goes on increasing till not the gate pulse is removed from the Q2. Also, since the diode D1 is reversed biased in this mode and the switch S1 is off, no current flows through the switch Q1.

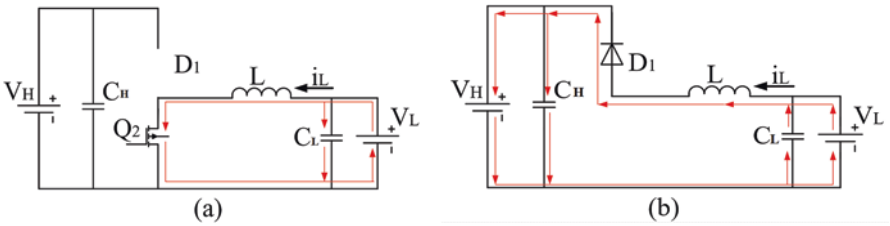

Fig. 4.13 Boost mode. (**a**) Interval 1, (**b**) Interval 2

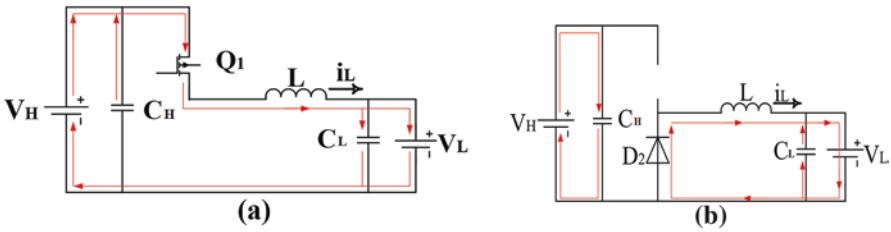

Fig. 4.14 Buck mode. (**a**) Interval 1, (**b**) Interval 2

Interval 2 (Q1-off, D1-on; Q2-off, D2-off) In this mode Fig. 4.13b, Q2 and Q1 both are off and hence can be considered to be open-circuited. Now since the current flowing through the inductor cannot change instantaneously, the polarity of the voltage across it reverses, and hence it starts acting in series with the input voltage. Therefore, the diode D1 is forward biased, and hence the inductor current charges the output capacitor C1 to a higher voltage. Therefore, the output voltage boosts up.

Mode 2 (Buck Mode) In this mode switch Q1 and diode D2 enter into conduction depending on the duty cycle, whereas the switch Q2 and diode D1 are off all the time. This mode can further be divided into two intervals depending on the conduction on the switch Q2 and diode D1 as shown in Fig 4.13a.

Interval 1 (Q1-on, D1-off; Q2-off, D2-off) In this mode Fig. 4.14a, Q1 is on and Q2 is off and hence the equivalent circuit is as shown in the figure below. The higher-voltage battery will charge the inductor and the output capacitor will get charged by it.

Interval 2 (Q1-off, D1-off; Q2-off, D2-on) In this mode Fig. 4.14b, Q2 and Q1 both are off. Again, since the inductor current cannot change instantaneously, it gets discharged through the freewheeling diode D2. The voltage across the load is stepped down as compared to the input voltage.

4.3 Simulation Results and Discussion of Stand-Alone PV System with BES

In this section, the dynamic performance of the PV system with BES during constant and variation of the solar irradiance is investigated. The temperature of PV array surface is considered to be constant at 25 °C during the entire simulation period. The PV array is rated 5 kW; MPPT control takes maximum power from PV using unidirectional DC/DC converter which is performed. The model designed in the previous parts is simulated in a Simulink environment which is illustrated in Fig. 4.15. The constructions of the system model to study the two cases are under constant and variable solar irradiation in different operating conditions. The chapter concentrates on the study of the impact of constancy or change in solar irradiation on the performance of BES. In the first case, the offered model works with constant solar irradiation and compares the results to the system in a case with and without BES. In the second case, the system works with variable solar irradiation. In both cases, the system is running in the same sequence. Initially, Load1 (3 kW) is run (*on*) and consumes more than half of the power generated by the PV system. After 1 second Load2 is running (*on*) making the total power consumed 6 kW. The PV system does not provide sufficient power; thus, supplemental energy is supplied by BES. This section also presents a consistent analysis of voltage and current after the filter using FFT tool. The load profile is connected to the system which is applied in all operating cases of the system as shown in Fig. 4.16. In the first operation case, a constant solar irradiation value (1000 W/m^2) is applied to the system. In the second operation case, the system is employed into the variable value of solar irradiation which appears in Fig. 4.21. The simulation is run for 4 sec. In the next section, the operating results of the model on the MATLAB/Simulink program for both cases and the effect on current, voltage, power, and harmonic analysis by FFT tools are presented.

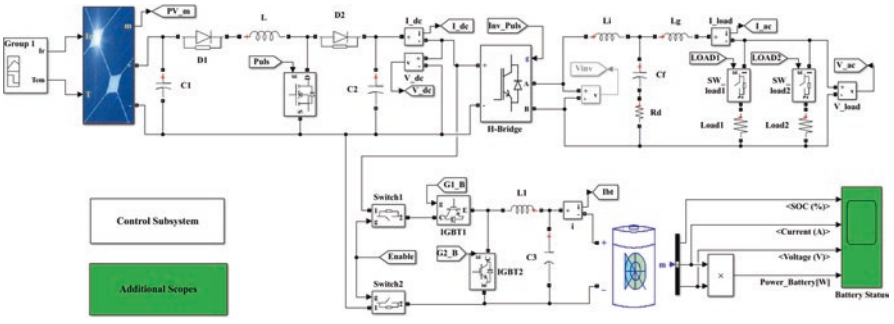

Fig. 4.15 Simulink model of a stand-alone PV system with a BES

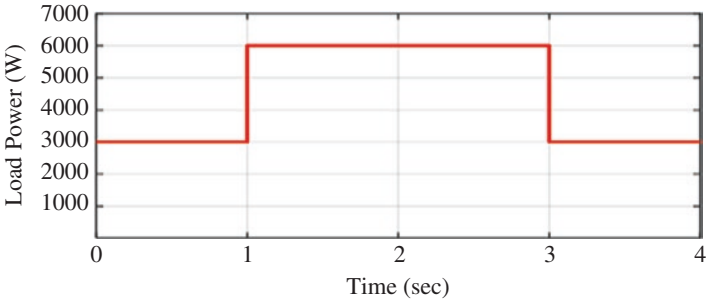

Fig. 4.16 Load profile

4.3.1 Comparison Between PV System with and Without BES Under Constant Irradiation

This subsection tackles the comparison of the operating results of the model in both cases with and without BES connected to the model. Comparison of the results of both cases is the focus of a set of important points: the amount of consumption when the load 1 is only in *on* situation, the entry and exit of the load 2, and the status of the system when there are loads that consume power more than what is generated by PV.

The current response of the PV system to the change in the load profile and with disconnecting and connecting the BES is illustrated in Fig. 4.17. As shown in Fig. 4.17a, there is no significant distinction in the current values of the PV for both cases. However, the output current of PV array (I_{pv}) is fairly constant at a value of 25 A if the BES is connected. At the start of operation, we notice that the current took a long time to settle at 25 A if no BES is connected to the system. However, it is observed that the current level is more stable when BES is used. Moreover, the existence of BES overcomes the effect of overshoot transient moments which result from the entry and exit of sudden loads. In Fig. 4.17b, when load 1 is only in *on* situation, it consumes a current of 19A in the case without BES. While the BES is connected, it consumes 14.7 A. This gives a 29.25% progress in the current. Transient moments resulting from the sudden entry of load 2 cause a current overshoot in the. The current overshoot approximately reaches 30.5% of the steady-state value in the first case. In the second case, the current overshoot approximately reaches 1% of the steady state of stability of the current. This improvement in the current also appears at the exit of load 2 and overcomes the undershoot.

Comparison of the voltage results for the two operating cases of the model is shown in Fig. 4.18. The result concludes that there is no significant difference in the PV voltage as illustrated in Fig. 4.18a but the overshoot at transient moments of the entry, exit of the load 2, and the starting of the model have been reduced. Illustrations, (b) and (c) of Fig. 4.18, show DC voltage and AC RMS load voltage which DC voltage (V_{dc}) stable at 280 V in the use of BES by suppressing or smoothing out transients that occur in PV systems.

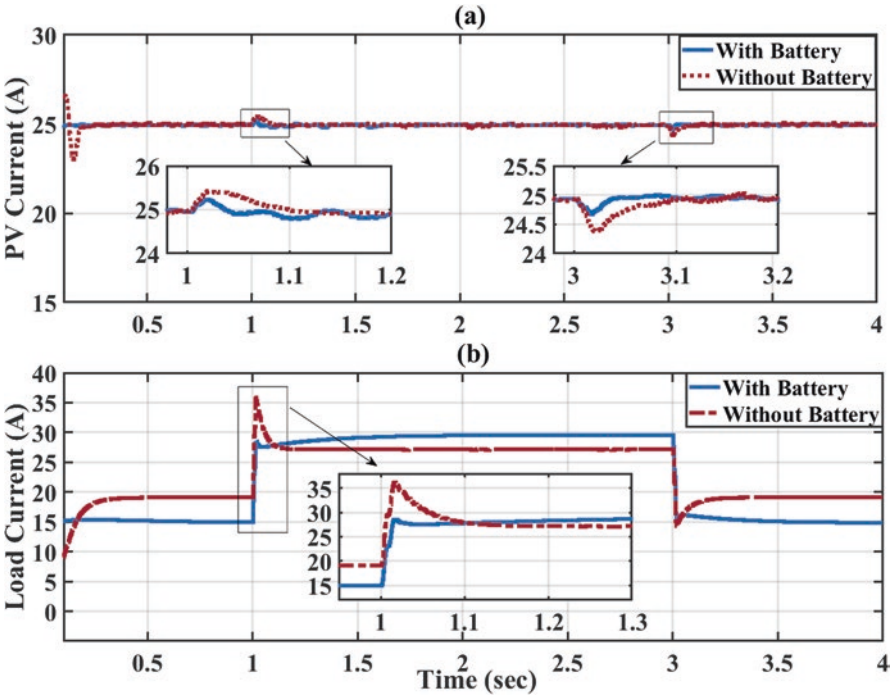

Fig. 4.17 The current response of PV system. (**a**) PV output current and (**b**) AC RMS load current

In the second case, when the load profile is changed from 3000 W to 6000 W, it leads to decrease in the DC voltage from 360 V to 256 V. Then, the DC voltage increases from 256 V to 360 V, in response to the change of the load profile from 6000 W to 3000 W, as illustrated in Fig. 4.18b. The AC voltage response at running the PV system without connecting BES are presented in Fig. 4.18c. The AC load voltage is decrease from 254.5 V to 181 V, when the load profile is changed from 3000 W to 6000 W. Then, the AC load voltage increases from 181 V to 254.5 V, in response to the change of the load profile from 6000 W to 3000 W.

The differences in current and voltage in two operating cases also appear when comparing the results of power as shown in Fig. 4.19. In order to evaluate the validation of the MPPT technique, Fig. 4.19a shows the output power of PV array (P_{pv}). It can be seen that the P&O MPPT technique can track accurately the MPP at 1000 W/m^2 of solar irradiance. Moreover, the impact of voltage and voltage stability is noticed during the use of the BES in power and provides the power consumed by each load according to need as much as possible. Relatively, the amount of power consumed in the system approaches 6 KW which is greater than what is generated by the PV array as shown in Fig. 4.19b.

The BES response for current, voltage, and SOC under the effect of the change in the load profile is shown in Fig. 4.20. When the model starts, the initial value of

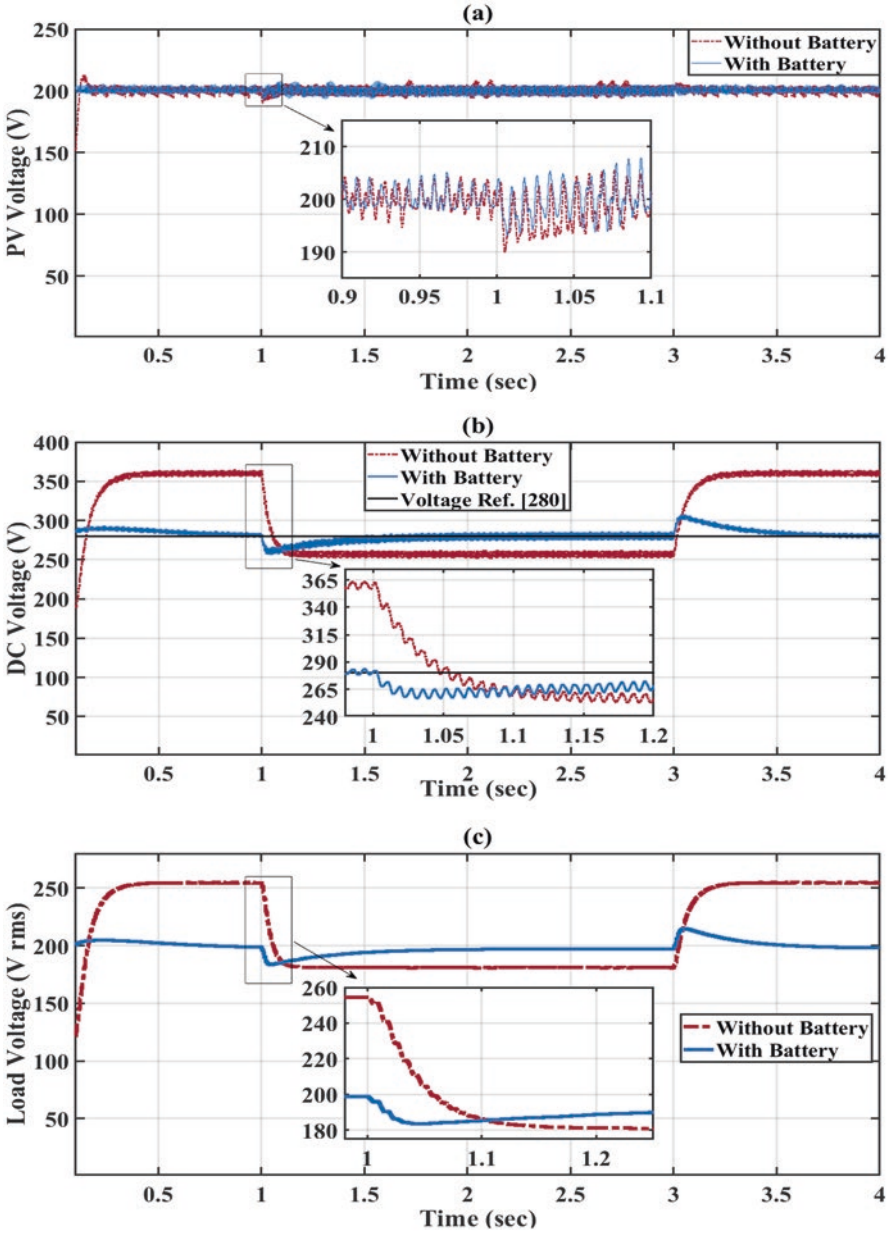

Fig. 4.18 The voltage response of PV system. (**a**) PV output voltage, (**b**) DC voltage, and (**c**) AC RMS load voltage

the profile is 3000 W, which is more than half of the power produced by the PV array, and thus the remaining power is about 2000 W. The remaining energy is charged by the BES as shown in Fig. 4.20a. When the load profile is changed from 3000 W to 6000 W, and this power is greater than what the PV array produce, the BES status switches from charge to discharge to compensate for the difference between the power required for the load and the power generated from the PV array. The change in BES status from charge to discharge shows an effect on SOC and voltage as illustrated in Fig. 4.20a, c. The change in the BES status effects on the battery current as its polarity changes from negative (charge) to positive (discharge) as shown in Fig. 4.20b. Then, the SOC and voltage increase again in response to the

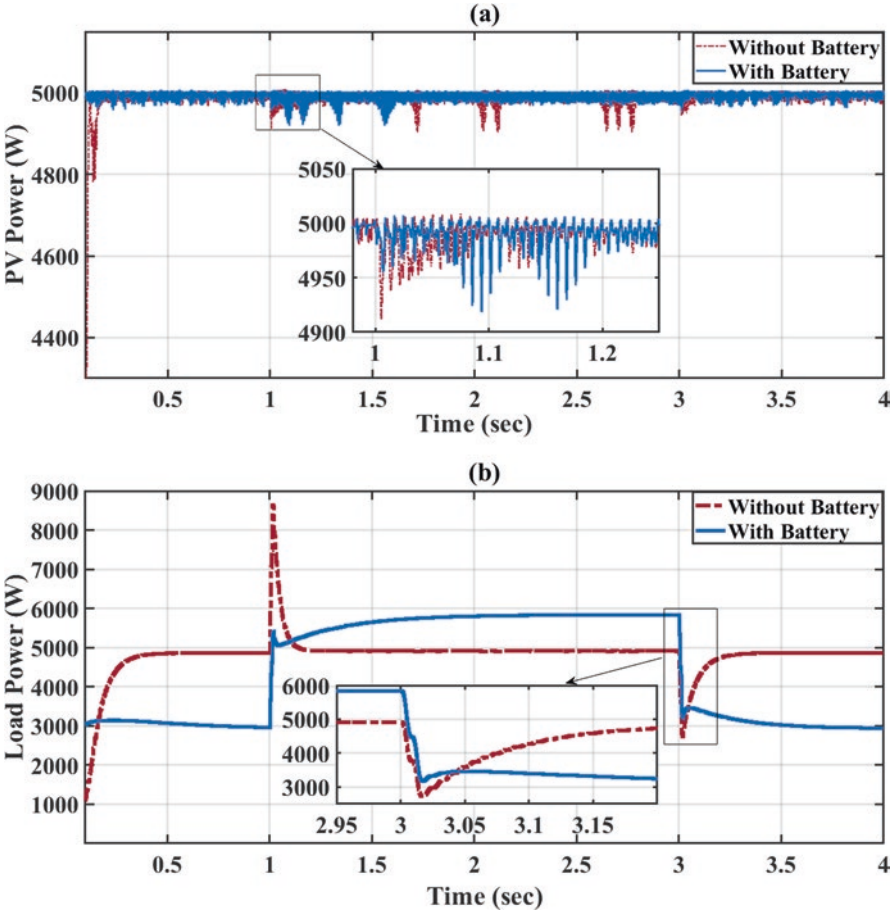

Fig. 4.19 The power response of PV system, (**a**) PV generated power, and (**b**) load active power

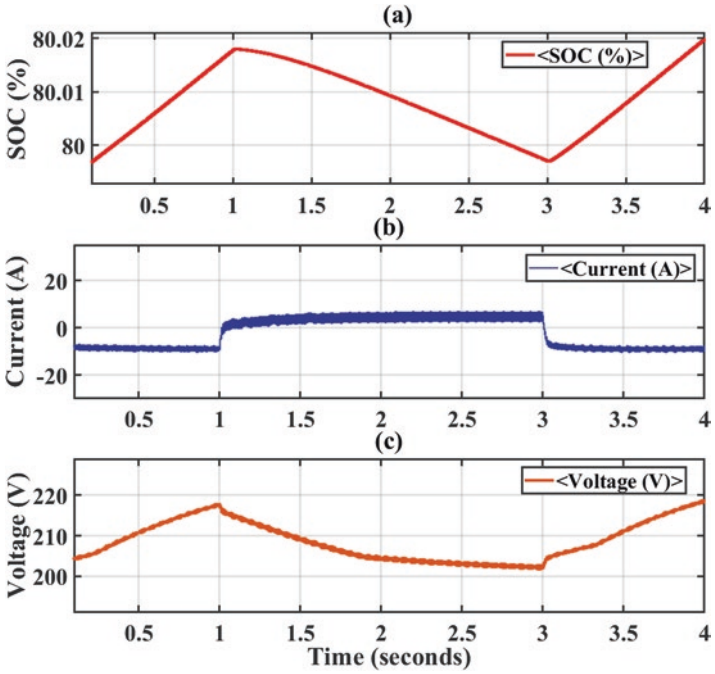

Fig. 4.20 The BES response. (**a**) Battery state of charge (SOC %), (**b**) battery current, and (**c**) battery voltage

change of the load profile from 6000 W to 3000 W. The current polarity returns back to a negative indication that the BES is charging.

4.3.2 Simulation Results PV System with BES at Variable Irradiation

In this subsection, the dynamic performance of the PV system with BES during variation of the solar irradiance is investigated. The temperature of PV array surface is considered to be constant at 25 °C during the entire simulation period. The solar irradiation profile appears in Fig. 4.21. This change represents a practical variation of solar irradiance during a complete one day as proposed in. The same scenario of load profile is applied in operating the system as shown in Fig. 4.16.

The simulation result for the current is represented in Fig. 4.22. Figure 4.22a illustrates that the output current of PV array (I_{pv}) reflects the variation in solar irradiance. When the solar irradiance is changed from 700 W/m^2 to 1000 W/m^2, it leads to increase in the output current of PV array from 17.5 A to 25 A. Then, the PV array current decreases from 25 A to 17.5 A, in response to the change of the solar irradiance from 1000 W/m^2 to 700 W/m^2. Variations in the AC curve Fig. 4.22b due to the

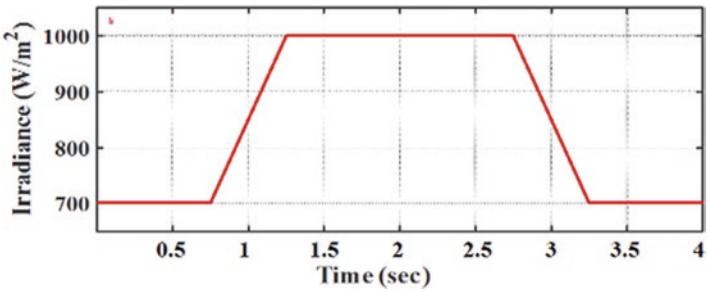

Fig. 4.21 Solar irradiation profile

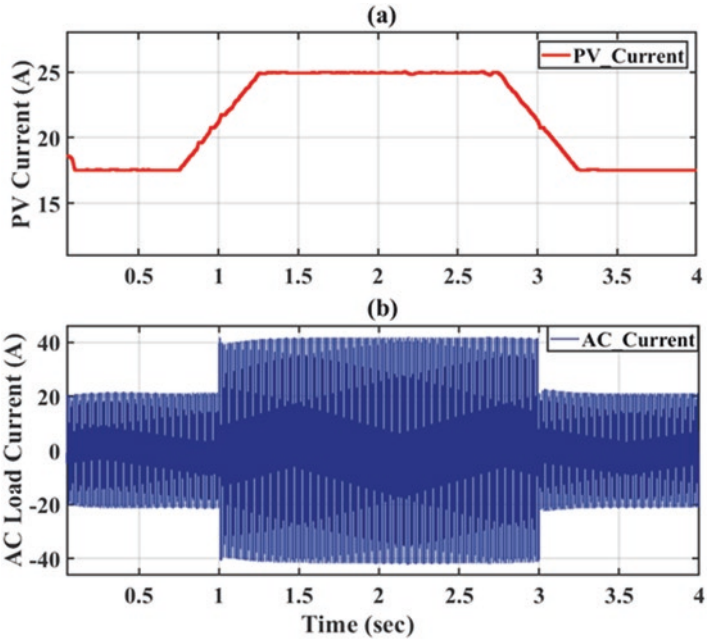

Fig. 4.22 Simulation results of the PV system with BES. (**a**) PV output current and (**b**) AC load current

sudden input of load 2 related to the model. When the load profile is changed from 3000 W to 6000 W, it leads to increase in the peak of AC current from 21.3 A to 41.85 A. Then, the AC load current peak decreases from 41.85 A to 21.3, in response to the change of the load profile from 6000 W to 3000 W, as illustrated in Fig. 4.22b. Also, the effect of change solar irradiance did not appear on the AC current due to the existence of a BES connected to the system, where the BES compensated the difference in the current to the load.

The output voltage of the PV array (V_{pv}) is maintained at 200 V as shown in Fig. 4.23a, despite the variation of solar irradiation. Therefore, the MPPT controller can accurately track the PV array voltage at the maximum power point (V_{mpp}) to harness the maximum power from the PV array during the rapid variation of solar irradiance. The proposed control on BES overcomes the transient moments resulting from the sudden switching of the load 2 and keeps up the value of the DC voltage level (output of the boost converter) at 280 V. Also, in Fig. 4.23b shows the stability of the AC voltage value. The BES compensated the voltage difference to stabilize the AC voltage on the load terminals.

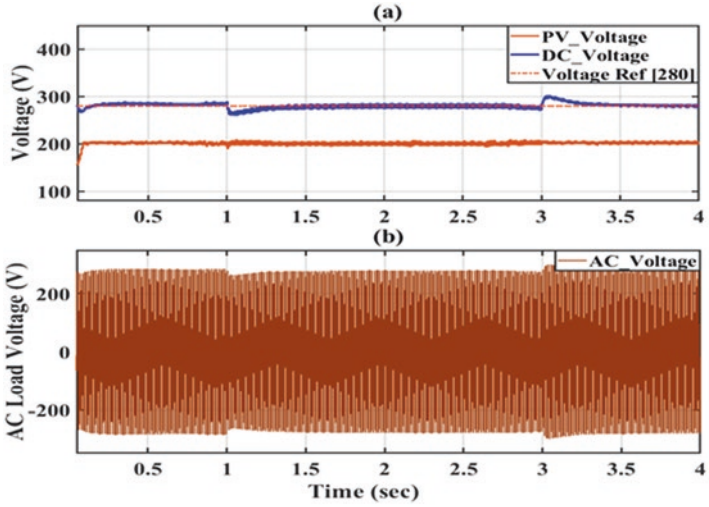

Fig. 4.23 Simulation results of the system with BES. (**a**) The PV output voltage and boost output DC voltage, (**b**) AC load voltage

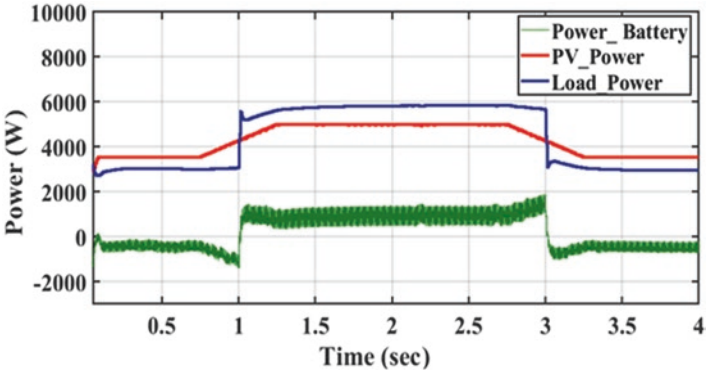

Fig. 4.24 Simulation results of the PV system without BES for the PV generated power, load power, and battery power

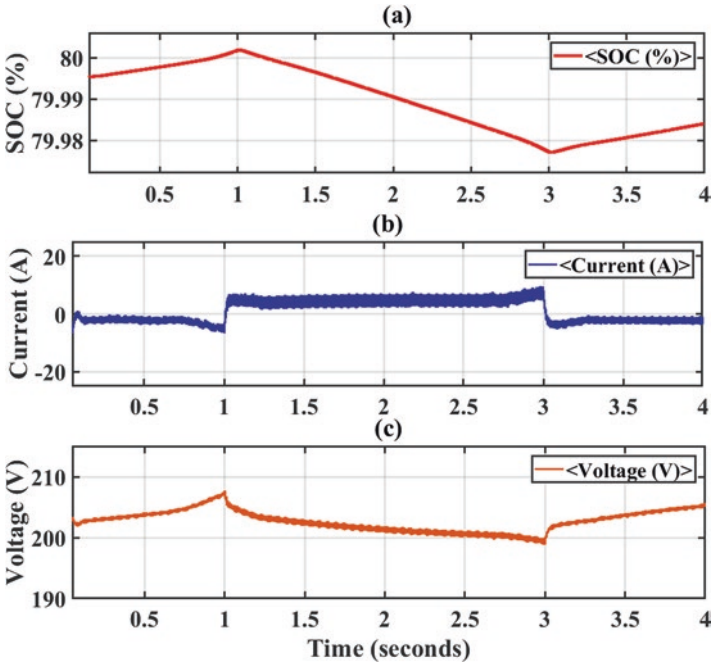

Fig. 4.25 BES response (**a**) SOC %, (**b**) battery current, and (**c**) battery voltage

In order to evaluate the validation of the MPPT technique, Fig. 4.24 shows the output power of one PV array (P_{pv}). It can be seen that the P&O MPPT technique can track accurately the MPP when the solar irradiance changes rapidly. Also, the figure shows the power of the BES and the power consumed by both loads during the system operation at the same scenario of load profile.

Figure 4.25 shows the operating curves of the battery (SOC, voltage, and current) under the effect of changing solar irradiation. In Fig 4.25a, the battery SOC varies depending on both solar radiation and load profile. In the case of an excess of power in the production of PV array, it is charged by BES. Conversely, in case of low power output from PV array, the BES will compensate for the difference in power to the load as show in Fig. 4.25b, c.

4.3.3 Voltage and Current Harmonic Analysis

The PV inverter should satisfy high power quality to meet standard recommendations of harmonics as dictated by national standards such as IEEE 519 and IEC 61727. The IEEE and IEC standards recommended that THD should be less than 5%, and the higher harmonic content of each individual harmonic is not more than 3% for PV system [84, 85]. The harmonic spectrum of both inverter voltage and

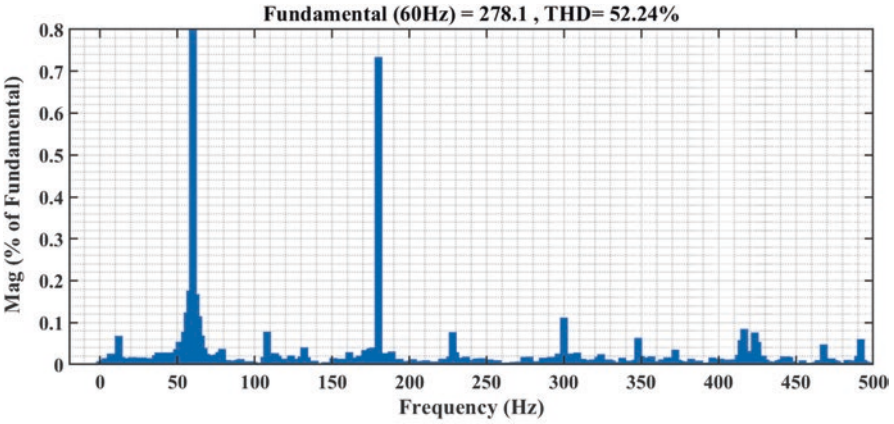

(a)

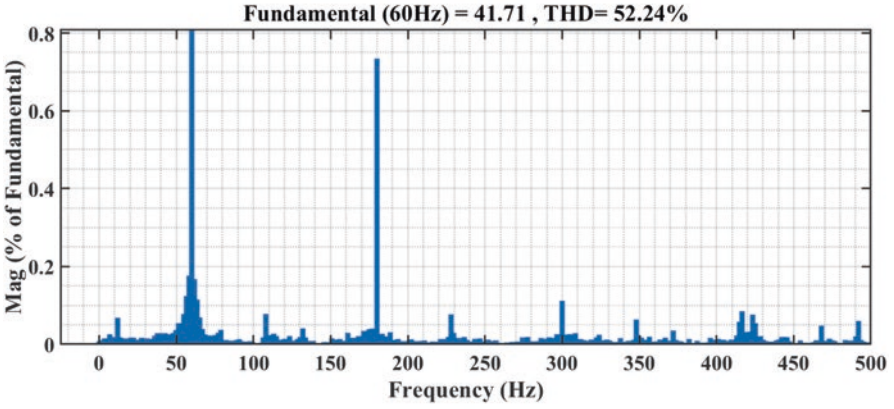

(b)

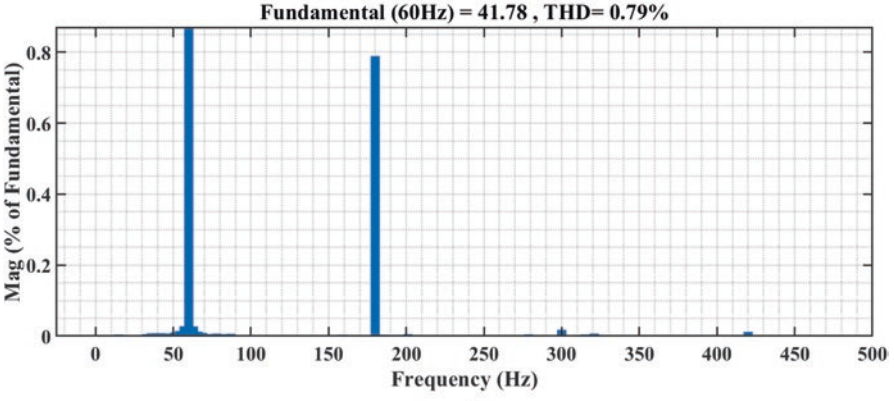

(c)

Fig. 4.26 Harmonic analysis of AC load current and AC load voltage before and after using LCL filter. (**a**) THD of the AC voltage before using LCL filter. (**b**) THD of the AC current before using LCL filter. (**c**) THD of the AC voltage after using LCL filter. (**d**) THD of the AC current after using LCL filter. (**e**) Harmonic spectrum of AC current after using LCL filter

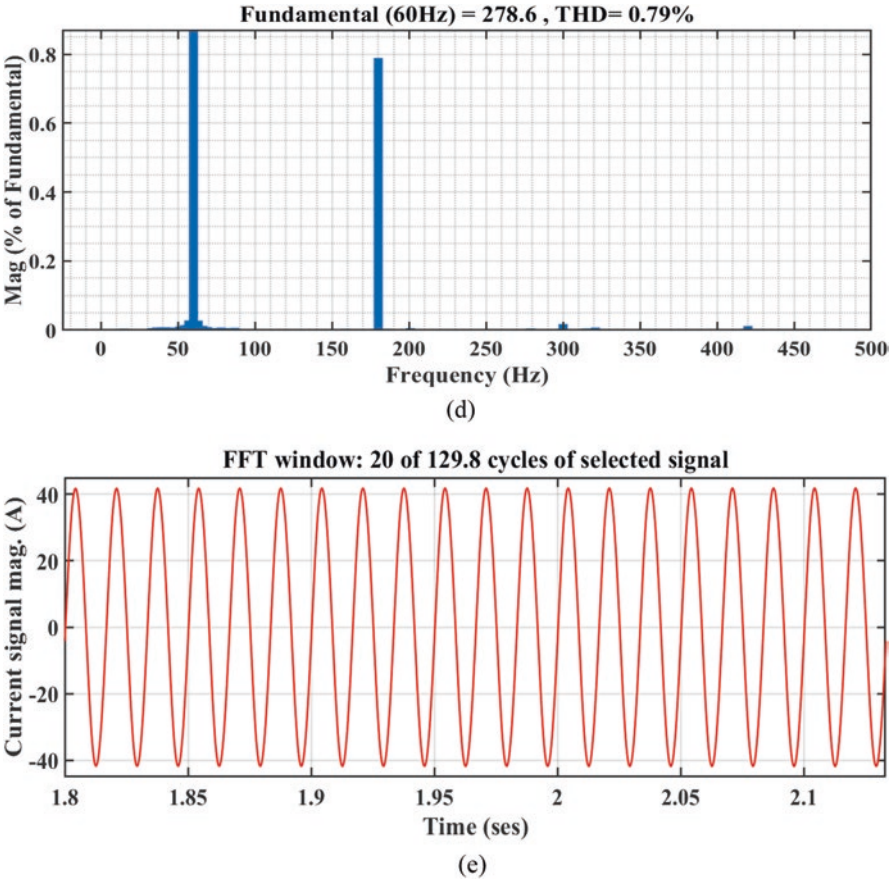

Fig. 4.26 (continued)

current of them after using LCL filter is shown in Fig. 4.26a, b. It shows the THD for both inverter voltage and current are 52.24%. The LCL filters are designed from a rating of the inverter and used to remove the harmonics which are generated from the inverter. Under steady-state operation, the voltage and current waveforms are taken to evaluate the harmonics control of the designed PV system. The standard tool in MATLAB for FFT tools is used to decide the harmonic magnitude of the AC voltage and AC current. Figure 4.26c, d shows the THD for both inverter voltage and current are 52.24% that after using LCL filter. The harmonic spectrum of AC load current after using LCL filter is shown in Fig. 4.26c.

4.4 Summary

This chapter investigated the dynamic performance of the studied PV system with BES during variation of the solar irradiance. Moreover, the effectiveness of the implemented MPPT techniques and the employed control strategy is evaluated during variations of the solar irradiance. This chapter is primarily intended to enhance the dynamic performance of the proposed PV system with BES under constant and variable solar irradiation. Furthermore, an optimal control strategy is presented. The proposed system targets in reducing the impact of transient moments resulting from the sudden entry and exit loads connected to the system. It also explains the role of the BES in how to manage system loads and demonstrates the improvement in the performance of PV systems. The system presented in the chapter is evaluated and compared to the traditional system without BES. The simulation results show that the capacity of the BES helps to improve the performance of the system through the control used in the process of loading and unloading to manage the sudden load changes and helps to maintain a stable voltage level on the load and PV terminals. It is worth to mention that the control scheme with BES ensures stable voltage and current levels and overcomes the transient spikes that appears on the AC load current.